Alma Mater Studiorum – Università di Bologna

DOTTORATO DI RICERCA IN

FISICA

Ciclo XXVIII

Settore Concorsuale di afferenza: 02/D1

Settore Scientifico disciplinare: FIS/07

Dose optimization in cardiovascular interventional radiology

Presentata da: Dott. Bianchini David

Coordinatore Dottorato — Prof. G. Castellani

Relatore — Prof. R. Zannoli

Esame finale anno 2016

Index

1. PREFACE

The present PhD thesis is composed of two scientific articles that summarize the results produced in the last three year of doctorate. The first paper is already published in 2015 on the Journal of Mechanics in Medicine and Biology. The second article in under review to be published on Heart Rhythm Journal. These papers summarize only a part of the results obtained in the research during the doctoral activities. The choice to submit the PhD thesis combining scientific articles is a choice shared internationally with the only goal of writing's time optimization.

The articles presented in this thesis treat two different aspects of the same problem in the context of the optimization in interventional radiology. Both works use innovative solutions and methods, implemented in dedicated software, giving interesting results in the medical physics field .

2. INTRODUCTION

The present work is contextualized in medical physics, the field of physics applied in medicine, which aims to improve the quality of care through the use of physical methods.

The radiology is a medical technique that use imaging representation of the patient morphology and physiopathology in order to support clinical decision. The x-ray imaging is one of many physical systems to bring patient information outside of the patient body. The x-ray beam, indeed, pass thru the patient creating a spatial distribution of photon absorption. This absorption is necessary in order to generate radiological contrast: this mean that the patient dose is ineluctable. The optimization effort, goal of the medical physics, is both related on the photons energy used, in relation of the absorber (patient), and related on the property of the detector in term of quantum efficiency.

The absorbed dose D_a is universally recognized as a physical quantity that correlate the ionization density with the biological damage. This is why the dosimetry is the most common physical dimension used in the optimization of radiological protocols. The correct evaluation of the cost, ie biological damage, compared to a benefit, or the diagnosis or treatment, allows the physician to make the best choice, with the scientific method based on measurable quantity.

Generally, for the radiologists, or in general for the doctors involved in radiological diagnostics, the detriment generated by the absorbed dose to the patient is considered a “second-order damage”. This is due the immediacy of benefit over harm on one hand and on the other hand on to the limited knowledge of the biological effects of low doses absorbed to the patients. In radiation therapy, where the harm and the benefit are evaluated with the same physical dimension, which is precisely the absorbed dose. This allows the radiation therapist, for a given clinical goal, to assess properly the need to radiation-induced detriment.

The present work is divided in two chapters, realized in scientific articles form. The common issue is the radiological optimization in cardiovascular interventional. The cardiovascular interventional radiology is the radiological technique of diagnostic imaging used in support to micro-invasive surgery through blood vessel. In general, in interventional radiology the physician takes surgical decisions on the basis of the image obtained through the projection of the absorption of an RX beam. A planar detector picks up the signal and integrate it in a defined time interval. Since the physical interaction between the x-ray photons and the patient is both photoelectric absorption and Compton scattering, the resolution of the obtained images strongly depend on the thickness of the patient, the energy spectrum and the relative distance between the focal spot, the patient and the detector. The scattered photons generate a noise over the absorption signal: in this perspective the Compton effect is the most unwanted effect in radiology.

It's known that the diagnostic image is the benefit for the patient, while the "cost" is the patient does. Recent international guidelines impose limits to the detriment induced by the interventional practice in term of fluoroscopy time, total dose area product (DAP) and entrance skin air kerma (ESAK).

The task of my work of medical physicist is to minimize the cost/benefit function related to the use or radiation on patient. In this context the research carried out in the course of my PhD is focused on the criteria for dose optimization in interventional cardiovascular procedures.

The cardiovascular imaging uses contrast medium (CM) in order to create contrast between blood vessels and surrounding tissue. The using of iodinated CM is limited due to side effects like induced nephropathy and allergic reactions. The digital technology revolution permits to use positive CMs, like carbon dioxide, that have weaker absorption contrast compared to Iodinated CM. A gas, in a pulsed flow of liquid, generate bubbles, that have geometrical dimension different to the blood vessels in study.

The greatest effort is to reproduce, in theory and in experiments , the variables representative of the patient in the context that is being analysed in the optimization studies. Since the standard patient does not exist, the statistical variability imposes an investigation case-dependent with big-data

analysis methods. In this optics there is an increasing interest on the evaluations of the efficacy of the optimization process based on the data recorded in the radiological databases. With this address the second paper presented in this thesis is oriented to address the dose optimization goal with the statistical analysis of structured data recorded in different databases present in hospitals.

3. CARBON DIOXIDE ANGIOGRAPHY: SIMULATION OF OPERATIVE CONDITIONS FOR DIAGNOSTIC IMAGE OPTIMIZATION.

Abstract: Carbon dioxide angiography is based on the visualization (i.e., the radiographic contrast) of gas bubbles injected in blood vessels. By using an experimental X-ray bench, it has been measured the energy response of a flat panel detector (Varian CB4030) and, with a dedicated phantom and a software simulation, the image contrast of vessels injected with Iodine and CO2. Moreover, the dynamical behaviour of a moving gas bubble has been studied with the software simulator. The results show that the contrast generated by carbon dioxide is about one fourth of that obtained with iodine, demonstrating that CO2 angiography should use different radiological settings with respect to iodine angiography. In particular, a kVp increase have a lower reduction of CNR with carbon dioxide than with iodinated CM, suggesting possible technological improvements both on radiological emission and image enhancement methods.

Key Words: CO2 Angiography, Interventional Radiology, Contrast Induced Nephropathy

Introduction

The increase of radiological medical procedures during the past two decades is clear, mainly in the field of interventional radiology, where a variety of procedures have a tremendously increased in number and complexity (1–3), involving patients with serious clinical conditions, such as renal impairment and allergies to iodinated contrast medium (CM). This last reason have supported research on the possibility to use an alternative contrast medium during

interventional procedure, such as carbon dioxide (CO2).

A previous work was focused on the biomechanical aspects involved in CO2 angiography, with great attention on gas flow control and possible damages at the vessel walls during the gas injection (4). The aim of this work is to study the radiological aspects of the procedures, when CO2 instead of iodine was used as contrast medium.

Despite typical liquid CM (i.e., iodine contrast medium), the visualization of a gas inside a vessel requires new considerations, related to the different dynamic behaviour and to the radiological characteristics (i.e. the differences in linear attenuation coefficient curves). In fact, while the iodine CM is mixed with blood and has a sharp k-edge absorption peak at photon energy of 33.2 keV, CO2 CM does not mix with blood but forms bubbles which move inside the vessel, changing the previous absorption of radiation by blood inside the lumen. Some authors describe the radiological effect produced by CO2 as a "negative contrast", referring to the characteristic of the CO2 to have a linear attenuation coefficients curve lower than that of the human tissues, in opposition to the "positive contrast" induced by iodine CM (5-6). This difference is used to explain the inverse grey levels of the imaged vessels filled with CO2 or iodine, but it is not stressed by X-ray machines. In fact, the pre-selected radiological parameters (i.e. voltage and current settings) during exposures seem to be not so different when iodine or CO2 CMs are used, limiting the possibilities to optimize CO2 images.

For these reasons, in this paper we present the rationale of a possible optimization of radiological CO2 imaging, analysing the results obtained by a simulation software and a phantom with vessels filled with CO2 and iodine contrast medium.

Methods

Starting from the ideas that optimization of CO2 angiography is based on image subtraction , low frame rate (2÷8 fps), long frame exposure (10÷30 ms) and successive images staking, our attention has been focused on the possibility

to improve the signal to noise ratio (SNR) of the obtained images by acting on these parameters (7).

A radiographic image consists on the visualization of local difference of signal produced by the propagation of photons from a focal spot, through an absorbing material, to a matrix of detectors. Due to the stochastic interaction of the photons with matter, the resultant image superimposes useful information (signal or contrast) and noise. The image contrast to noise ratio (CNR) can be defined as the difference in mean signal of two adjacent regions of a planar image divided by the variability of the mean signal(8) and could be used as a sensitive parameter to compare different operating settings. Therefore, to have diagnostic information within a region with contrast medium and its surround, there must be a difference of mean signal greater than the statistical noise.

The simulation of this process is not simple because the linear attenuation coefficient of a medium depends on the energy of the photons and the X-ray tube produces a photon beam with a wide energy distribution (X-ray spectrum), related to tube voltage and current. For this, to compare the absorption by tissue and contrast medium (iodine or CO2) it is necessary to know the X-ray spectrum and calculate the global effect integrating on the energy base (9).

To calculate the changing in CNR with radiological parameters (kV, mA, timing) we developed a Labview ® simulation program. The software generates a virtual radiological X-ray beam with an energy spectrum obtained by Poludniowski (10) algorithm. Starting from this X-ray spectrum, interposing a phantom of known tissues depths and using the Lambert Beer formula attenuation law, it was possible to analytically calculate the X-ray intensity and spectrum on each point of a detector surface.

In order to convert the photons interacting with each detector pixel in a radiographic signal, it is necessary to introduce a transfer function that represent the detector response and the efficiency function (8). The EAE (Energy Absorption Efficiency) function expressed in "Eq. 1" permits to calculate the efficiency coefficient related to the energy of a photon interacting with a particular detector thickness:

$$EAE(E) = \left(\frac{\mu_{En}(E)}{\mu_{abs}(E)}\right) * \left(1 - e^{-\mu_{abs}(E)*x}\right) \qquad (1)$$

where μ is the linear attenuation coefficient of the detector materials (divided in absorption and energy transfer components) and x its thickness.

A signal noise is added to the generated spectrum. This operation is mandatory for the comparison of the SNR simulated (11). The noise has been calculated as the standard deviation of Poisson distribution of the number of photons in each energy interval ($\sigma=\sqrt{N}$) (8).

Difference in x-ray absorption between iodine and C02 CMs.

The physical contrast of an object in a surrounding material is directly derived from the exponential attenuation (Beer-Lambert law). In particular, the ratio between two contrasts can give a direct comparison of two CMs (Equation 2).

$$Contrast\ ratio = \frac{I_{Iod} - I_{Tissue}}{I_{Co2} - I_{Tissue}} = \frac{e^{-\mu_{Iod}x} - e^{-\mu_{Tissue}x}}{e^{-\mu_{Co2}x} - e^{-\mu_{Tissue}x}} \qquad (2)$$

Where *I* is the intensity passed thru the material and μ it's attenuation coefficient. The iodated CM (350mg/ml) has a density of 1.27g/cm^3 and is made for the 27% of iodine and for the 73% of water. The attenuation values of this mixture are taken from the NIST. The evaluation of the contrast ratio of 0.5mm CMs is displayed is Figure 2. In the same figure is also presented the energy spectrum of a typical medical system (80kV, 3,1mmAl HVL, 33.1KeV Mean Energy).

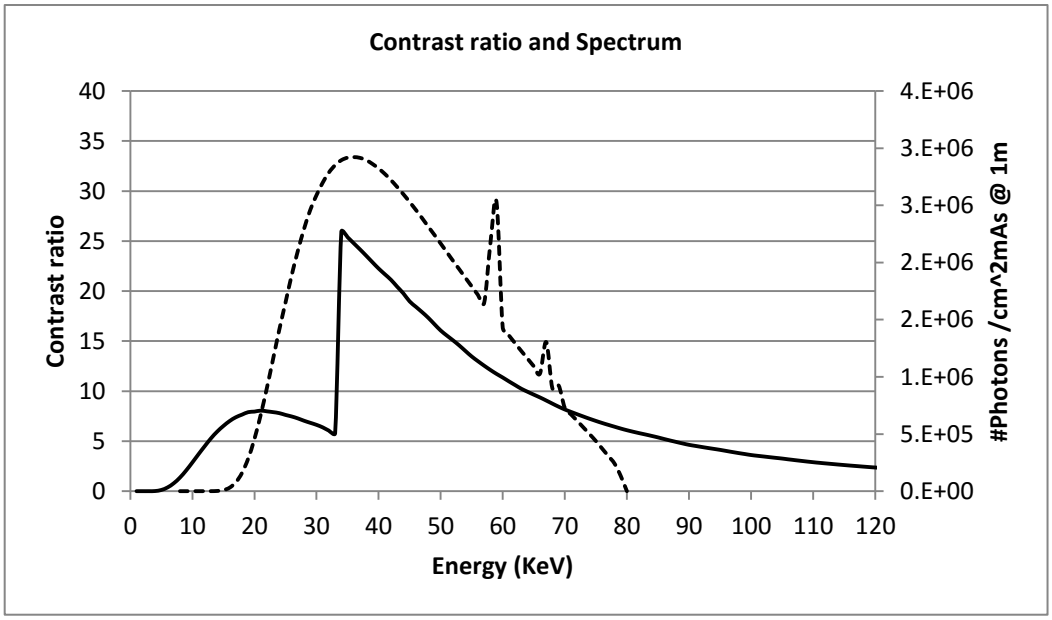

*Figure 2: Continuous line: Contrast ratio (Eq 2) between Iodine (350mg/ml) CM and CO2 respect to Tissue(ICRU44). Dashed line the spectrum for a 100kVp 5mmAl in N/(cm^2*s).*

Experimental setup

In order to compare the images obtained with the x-ray software simulator with the real x-ray images, a dedicated experimental setup with X-ray source, phantom and image detector was used . In this way it has been possible to measure the real CNR on radiographic images obtained with different CMs thickness and to simulate the same condition with software. The measures were taken with an optical bench equipped with a medical HF generator (SIAS Bologna) coupled with an X-ray tube (IAE RTM70H). The detector was a Varian CB4030 with squared pixel of 194µm CsI scintillators . The detector response was linear in dose (R^2=0.99) and the detector noise was proportional to the root square of the number of photons (R^2=0.99).

The contrast of the CMs has been measured with a dedicated plastic phantom made with 25x25 PMMA slabs of 15cm total thickness. The middle slab has been shaped with different inserts to have two regions with steps of different thickness from 0.5mm to 5mm. One region has been filled with Iodinated CM (350mg/ml) and the other region has been filled with ambient pressure air to

simulate Co2. In each thickness region an image ROI (1288pixels) was outlined and the mean pixels value and the standard deviation were calculated (Figure 3)

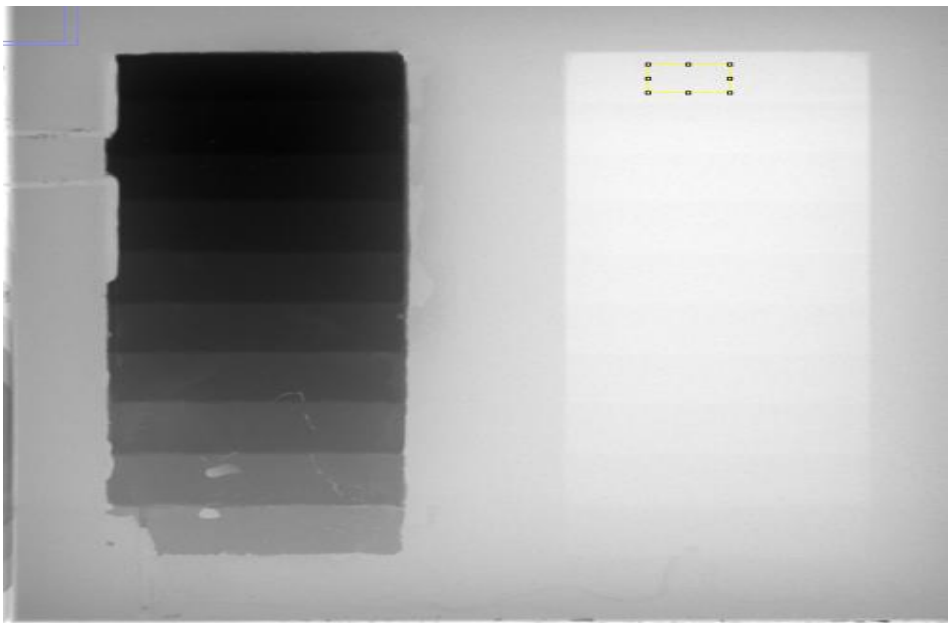

Figure 3: Radiographic image of the phantom. Left side iodine CM, right side air. From top to bottom steps from 5mm to 0.5mm.

The relative energies absorbed by the detector have been evaluated with the EAE function for each spectrum and the simulated pixels value has been evaluated using the formula expressed in Eq. 3.

$$Pixel_{value} = \sum_{Emin}^{Emax} EAE(E) * N(E) \qquad (3)$$

The software simulation calculated the photons absorbed basing on the photons number in each spectrum bin that interact on each pixel. The map of the total absorbed energy was multiplied for a gain factor in order to compare the simulated values with the measured grey levels.

Results

In Fig. 4 the comparison of the acquired and the simulated image for different kVp settings is shown.

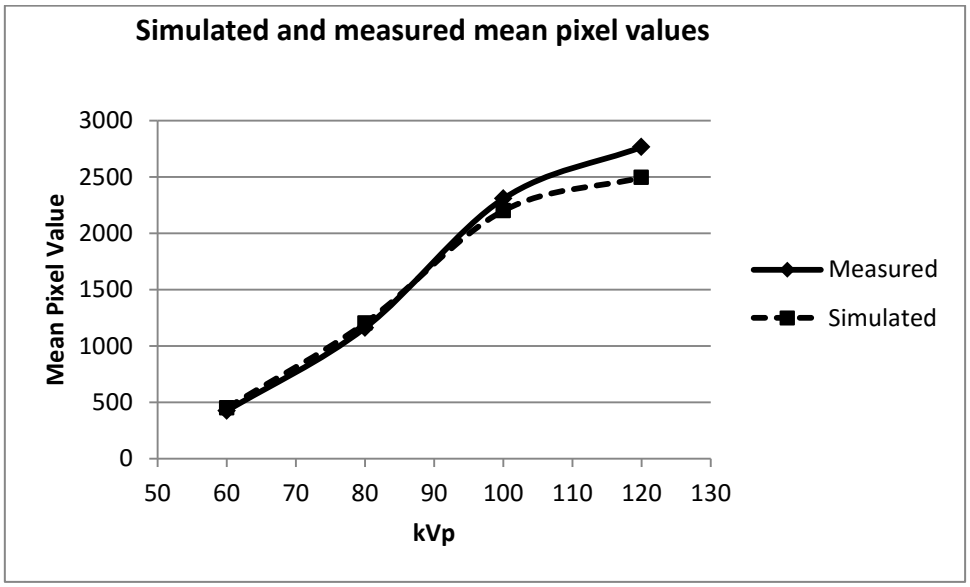

Figure4: Mean pixel value of simulated (dashed line) and measured pixel value (continuous line)

In Fig. 5 are presented the CNR for different kVp obtained with Iodine 350 CM and CO2 CM in different thickness.

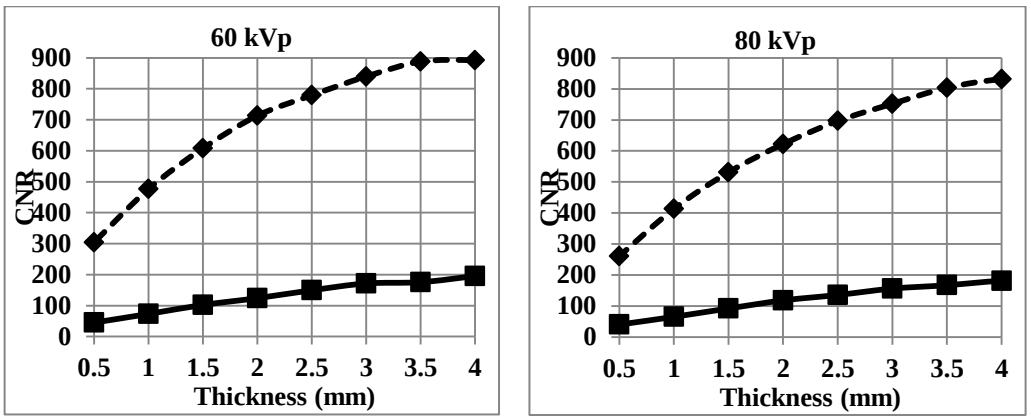

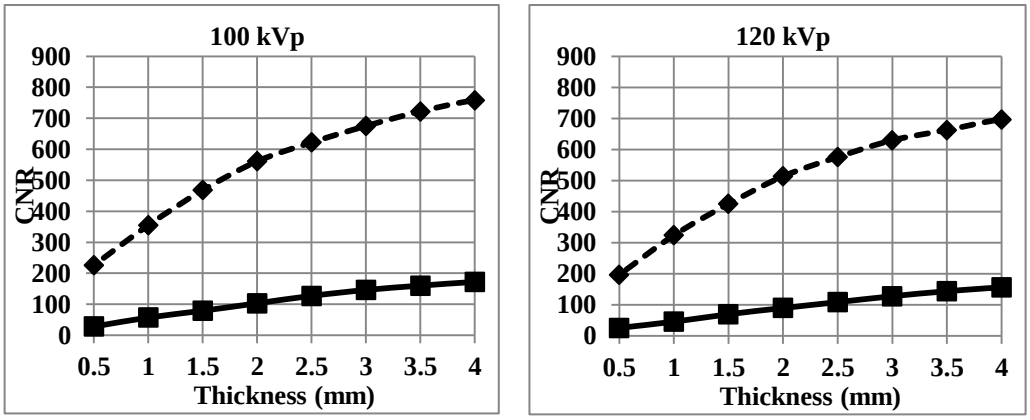

Figure 5: CNR measured for different thickness of CM: CO2 in continuous line and iodine CM in dashed line.

As described the software simulation has been set in order to respond as the real detector. The changing of CNR due to an increase of kVp has been calculated for 0.15 mm thickness (Fig. 6).

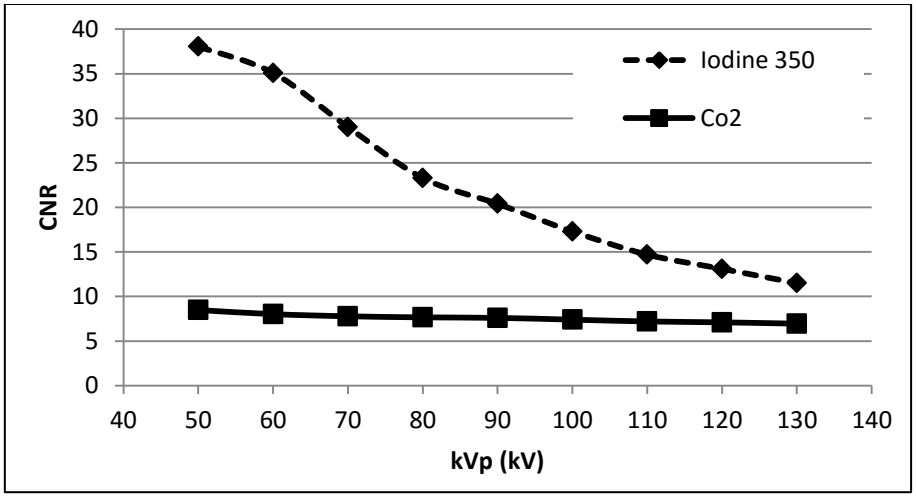

Figure 6: *Voltage dependence of simulated 0.15 mm CM object visualization . CO2 in continuous line and iodine CM in dashed line.*

Discussion and Conclusions

CO2 angiography is rapidly increasing his application rate, due to changes in

patients population (age , diabetes, renal failure) and availability of new semi-automatic gas injectors (12-13) . Nevertheless, the radiological approach to the interventional procedures doesn't significally changed and on this side it is possible to improve the quality of diagnostic result. For this reason it is necessary to optimize the radiological dose management and the enhancement of the image quality, which depends on contrast medium visualization and noise reduction. A validated computer simulation program may be very useful to observe how the signal to noise ratio changes in the different operative conditions .

The first aspect to discuss is the comparison of image contrast response for CO2 and Iodine. From Fig. 5 it is clear that the image contrast obtained with iodine is about four times higher than that obtained with CO2. We can compensate this difference by increasing the radiation dose when using CO2 or by optimizing the procedural aspects. On this second side we have a lot to do by changing gas bubble mechanics, frame rate and frame exposure time.

The second important aspect which emerge from the simulation is showed in Fig 6 . representing the contrast to noise ratio for Iodine and CO2 , with respect to X-ray tube voltage.

It is clear from the figure that the SNR for iodine is always higher than that of CO2 (and we must try to compensate the difference by acting on the X-ray dose and on the procedure), but SNR of Iodine sharply decreases with voltage while that of CO2 is quite stable. This may appear an useless evidence but on the side of the radiological technology it may have great importance. In fact the complexity and the cost of an angiographic apparatus is strictly related to the power of the X-ray generator and to the X-ray tube current. With iodine it is necessary to use limited voltages and high currents, to have most part of the photons in the iodine k-edge range (33.2keV), so increasing the tube current and power. With CO2, there is no k-edge and it is possible to increase the voltage to compensate the increase of current, with lower generator and X-ray tube power. It is not so simple, because the voltage increase has a direct effect on Compton diffused radiation, and the net benefit has to be accurately evaluated, but it is an interesting direction to move.

References

1. Persson, P. B., Hansell, P., Liss, P., Pathophysiology of contrast medium–induced nephropathy. *Kidney international*, *68*(1), 14-22, 2005.
2. Goodney, P. P., Tarulli, M., Faerber, A. E., Schanzer, A., Zwolak, R. M. , Fifteen-Year Trends in Lower Limb Amputation, Revascularization, and Preventive Measures Among Medicare Patients. *JAMA surgery*, 2014.
3. Stacul, F., Van der Molen, A. J., Reimer, P., Webb, J. A., Thomsen, H. S., Morcos, S. K., Contrast Media Safety Committee of European Society of Urogenital Radiology (ESUR. (2011). Contrast induced nephropathy: updated ESUR contrast media safety committee guidelines. *European radiology*, *21*(12), 2527-2541, 2011.
4. Corazza, I., Rossi, P. L., Feliciani, G., Pisani, L., Zannoli, S., & Zannoli, R., Mechanical aspects of CO 2 angiography. *Physica Medica*, *29*(1), 33-38, 2013.
5. Hawkins, I. F., Wilcox, C. S., Kerns, S. R., & Sabatelli, F. W. CO 2 digital angiography: a safer contrast agent for renal vascular imaging?.*American journal of kidney diseases*, *24*(4), 685-694, 1994.
6. Shaw, D. R., Kessel, D. O. The current status of the use of carbon dioxide in diagnostic and interventional angiographic procedures.*Cardiovascular and interventional radiology*, *29*(3), 323-331, 2006.
7. Moresco, K. P., Patel, N. H., Namyslowski, Y., Shah, H., Johnson, M. S., & Trerotola, S. O., Carbon dioxide angiography of the transplanted kidney: technical considerations and imaging findings. *AJR. American journal of roentgenology*, *171*(5), 1271-1276, 1998.
8. Beutel, Jacob, Harold L. Kundel, and Richard L. Van Metter. *Handbook of Medical Imaging, volume 1: Physics and Psychophysics*., 2000.
9. Baldazzi, Rossi P.L., Masetti S., Turco A., Fiaschetti M., Lanconelli N., Bianchini D., Roma L., Nicoletti G., Lollini P.L., Characterization of biological tissues using X-ray attenuation data. *Nuclear Science Symposium Conference Record, 2008. NSS'08. IEEE*. IEEE, 2008.
10. Poludniowski, Gavin G. Calculation of x-ray spectra emerging from an x-ray tube. Part II. X-ray production and filtration in x-ray targets. *Medical physics* 34.6, 2175-2186, 2007.

11. Sandborg, M., Dance, D. R., Persliden, J., & Carlsson, G. A., A Monte Carlo program for the calculation of contrast, noise and absorbed dose in diagnostic radiology. *Computer methods and programs in biomedicine*, *42*(3), 167-180, 1994.
12. Novelli, Eugenio. "What's Trending." *J INVASIVE CARDIOL* 27.1, 20-26, 2015.
13. Scalise, F., Novelli, E., Auguadro, C., Casali, V., Manfredi, M., & Zannoli, R., Automated carbon dioxide digital angiography for lower-limb arterial disease evaluation: safety assessment and comparison with standard iodinated contrast media angiography. *The Journal of invasive cardiology*, *27*(1), 20-26, 2015.

4. PATIENT DOSE REDUCTION IN CARDIAC EP PROCEDURES FOLLOWING THE IMPLEMENTATION OF IMAGE NOISE REDUTCION TECHNOLOGY

Abstract

The aim of this work has been to evaluate the patient dose comparison between before and after the introduction of the Philips Clarity system upgrade. The retrospective study has been made on 561 procedures of pacemaker (PM) and implantable cardioverter defibrillator (ICD) implantations (134 pre, 192 post), and 235 procedures of radio frequency ablation (RFA) procedures (91 pre, 144 post). The pre and post sets are compared over clinical details in order to define an average patient for each intervention type. Each procedure has been studied over single irradiation event collected in the Structure Dose Report (SDR). The dosimetric quantities taken in consideration are the Dose-Area Product (P_{kA}) and the Interventional Reference Point Dose (IRP). These cumulative quantities are not normal distributed over a single procedure type, so a log-normal hypothesis has been made for the evaluation of the mean and the confidence intervals. The results shows a significant reduction of the for the DAP equal to 54% over all the procedures. The total fluoroscopy time didn't change appreciably and this shows in first instance that that the subjective image quality didn't change too.

Introduction

It has long been recognised that complex cardiac electrophysiology [EP] procedures such as RF ablation employ long periods of fluoroscopy, potentially leading to high patient radiation dose and, consequently, high staff doses [1,2]. Recent international guidance [3,4] and changes to international guidance and potential changes to EU regulation on eye dose limits along with the well-established concept of the 'as low as reasonable achievable' [ALARA] principle

have led to a growing interest in the optimisation of the balance between image quality and patient radiation dose in interventional procedures [5].

To that end, recent developments in image processing power that utilise Graphical Processing Units [GPUs] for advanced parallel processing of images have enabled real-time improvements in noise reduction in turn leading to the potential for reduced x-ray flux to the image detector[6–8] to achieve equivalent image quality. This could lead to a patient dose reduction in the clinical setting. An upgrade installation in the EP facility at Nottingham University Hospitals, Nottingham, UK [Allura FD10 Clarity; Philips, Best, Netherlands] enabled a population study to be conducted on patients undergoing EP procedures to compare radiation dose descriptors prior to the upgrade to those following the upgrade. This had the advantage of comparing procedures carried out on a similar case-mix of patients delivered by the same staff, thus minimising confounding effects on dose metrics that already have a distribution skewed towards high dose, with an attendant high variance. Therefore the objective of this study was to compare the radiation dose delivered for various EP lab procedures before and after the implementation of noise reduction software.

Methods

The present work is a retrospective single center study considering the improvements due the update of the x-ray equipment. The hypothesis that this work want to prove is the reduction of the patient dose (related to KAP and D_{AK})[9] and the unchanging of the Image Quality[7]. As image quality was not measured directly in this study, we used fluoroscopy time as an indirect metric related to the cardiologists' ability to conduct the clinical procedure. The patients' characteristics (Age and BMI), the procedures methods and operators team do not change significantly between before and after the update.

The x-ray equipment utilised in this study was a single-plane C-Arm cardiac x-ray unit [Alura FD10, Philips Healthcare, Netherlands] that was upgraded with image processing software incorporating the new noise reduction algorithms. The upgrade also involved retuned kV, mA and pulse width control curves associated with reduced detector dose requests and added filtration.

All the procedures are performed by experienced operators and the physicians team haven't changing during the period considered.

The using of algorithms in the image noise reduction for fluoroscopy systems in terms of spatial and temporal filters in order to maintain the same image quality with a reduction of x-ray energy fluence are presented in literature. [6,7]

Data relating to patient radiation dose, procedures and patients were collected. Patient radiation dose metrics collected were dose-area product [DAP], total fluoroscopy time and cumulative reference air kerma [D_{AK}] and were collected from the DICOM Modality Performed Procedure Step [MPPS] file sent to the Cardiology Image Archive server [Medcon, US] or the DICOM Radiation Dose Structured Report [RDSR] sent from the x-ray equipment. Procures were broken down into main procedure type [e.g. Pacemaker Implant] and, where numbers permitted, secondary procedure type [e.g. dual-chamber implant]. Procedural data were collected both from the radiation reports and also the Cardiology Information System [CIS] [Philips CVIS, Best, Netherlands], whilst patient data were collected from the CIS. Procedural data were collected to enable sub-division of dose metric analysis and patient data were collected to demonstrate the equivalence of the patient cohort for the before and after upgrade groups. The procedures are filtered in order to compare only the successful ones. The number of the procedures excluded do not bias the sampling as it is based only on clinical occurrences and the dropout rate is investigated.

Procedures

The subset of EP procedures analysed in the present work are the first nine in the dataset in order of sample size. This number is chosen to permit a statistically significant comparison between before and after Clarity update.

The procedure analysed are divided on main procedure, Pace Maker (PM) & Implantable Cardioverter Defibrillator (ICD) and Radiofrequency Ablation (RF) each of which is divide in sub-categories as follow:

- Pace Maker (PM) & Implantable Cardioverter Defibrillator (ICD) implant:

- Single Chamber PM - New implant;
- Dual Chamber PM - New implant;
- Single chamber ICD - New implant;
- Dual chamber ICD - New implant;
- Bi-ventricular ICD - New implant;

- Radiofrequency Ablation (RFA):

  - RFA - Atrial filbrillation (AFib) - Paroxysmal with Transoesophageal echocardiography (TOE);
  - RFA - Atrial flutter (common type);
  - RFA – Atrioventricular (AV) nodal slow pathway in Atrioventricular Nodal Reentrant Tachycardia (AVNRT);
  - RFA - Overt accessory pathway ;

The sub-procedures type are not selected on the basis of any other parameters if not on the basis of the total number of procedure collected in the databases. The clinical outcome of the intervention, like the occurrence of complications or patient death, or other bias variable, as interruption or procedure changing in course, is considered in the analysis.

Statistical analysis

The complexity of an interventional procedure is well shown in the variability of the duration between procedures of the same type[10,11], and the highly skewed distribution of variables. This is well known for cumulative quantities, such as Fluoroscopy time and DAP, that are made on the sum over single steps that compose the procedure. The hypothesis that can be made to explain the non-normality, can be the dependency of each clinical step error on the past clinical steps, so the error propagate in multiplicative way instead additive way[12]. This generate a natural skewed distribution known as log-normal distribution that characterize fluoroscopy time and dose in many other works[11,13]. Since there

isn't a robust log-normality test[14], in this work it will be only presented the the log-log Q-Q plot. The data comparison are made with non-parametric Mann-Witney U test with 1-tailed exact solution for DAP, D_{AK} , and 2-tailed exact solution for fluoroscopy time. On the mean value were evaluated the parametric 95% confidence intervals for a log-normal distribution as defined by Cox [15] although in the literature there are other methods used and a detailed scored comparison is not defined[14,16]. The discrepancy of Cox's method mean value from the median value convince us to use the 95% CI's on the median evaluated with the non-parametric Bonett & Price method[17]. Both the patients age and BMI distributions for pre- and post-update procedures are not-normally distributed as it is shown by the Shapiro&Wilk test (Shapiro & Wilk, 1965) ($p<.001$). This condition do not allow the using of the ANOVA homogeneity test. The equality of variance between the two groups is therefore proved with a non-parametric ranked Levene's test ($p>.05$). Statistical evaluations and tests are calculated using the SPSS software (IBM Corp, NY City, U.S.).

Results

The total number of procedures recorded for all the described intervention type is 588 of which 236 before the upgrade 352 after the upgrade. Due to clinical complications some of them are dropout and this reduce the cohort to 561 (-4,6%) of which 225 (-4.7%) before and 336 (-4,5%) after. This indicates that there was no difference with procedure completion rates before or after the image processing software upgrade.

Patients demographic

The patient demographic in pre update and post update is presented in Table 1. In table 1 is reported in the last column the p-value of the comparison between before update and after update evaluated with the Levene's method. The difference in sample density in the BMI comparison is due the CVIS database manual recording.

		Reference Before Update	After Update	Levene's p-value
Patient cohort	Total	225	336	
Patient Gender	Male	131 (58%)	212 (63%)	
	Female	94 (42%)	124 (37%)	
Patient Age (Years)	Measured on #	225	336	0.34
	Median (Min - Max)	67.0 (18 – 100)	67 (16 – 97)	
	Average (SD σ)	65.8 (17.8)	63.3 (17.8)	
	Asymmetry (SE)	-0.60 (0.16)	-0.66 (0.13)	
	Kurtosis (SE)	-0.12 (0.32)	-0.35 (0.27)	
Patient BMI (Kg/m^2)	Measured on #	41	51	0.18
	Median (Min - Max)	25.8 (20.3 - 70.4)	27.6 (18.9 - 46.1)	
	Average (sd σ)	28.8 (8.9)	29.6 (5.9)	
	Asymmetry	2.95	0.51	
	Kurtosis	11.51	-0.14	

Table 1: The patient demographic divided in pre update and post update

In figure 1 is presented the histogram of frequency distribution of the patient age. The data are presented to monitor the changing in patient age over the measure in different time, since there can be some shift due changing in eligibility criteria.

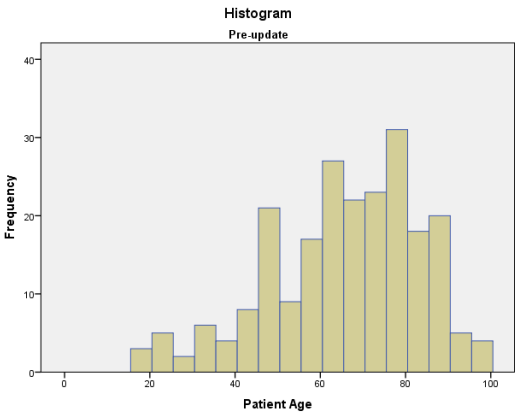

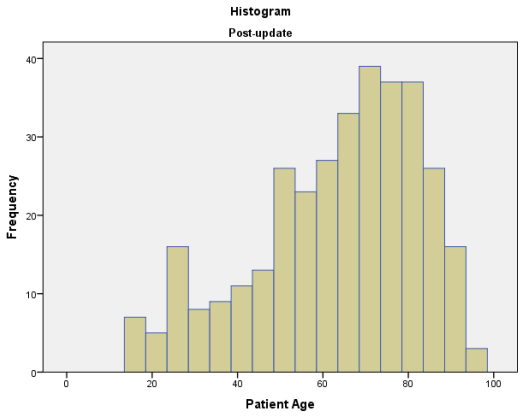

Shapiro-Wilk test p <0,001	Shapiro-Wilk test p <0,001

Figure 1: Frequency histograms of the patient age

In figure 2 are presented the BMI frequency distributions over all the cohort. The Shapiro-Wilk test gives a p-value p <0,001. The assumption of normality cannot be used and must be avoided in the median estimates of biometric parameters while defining the standard patient.

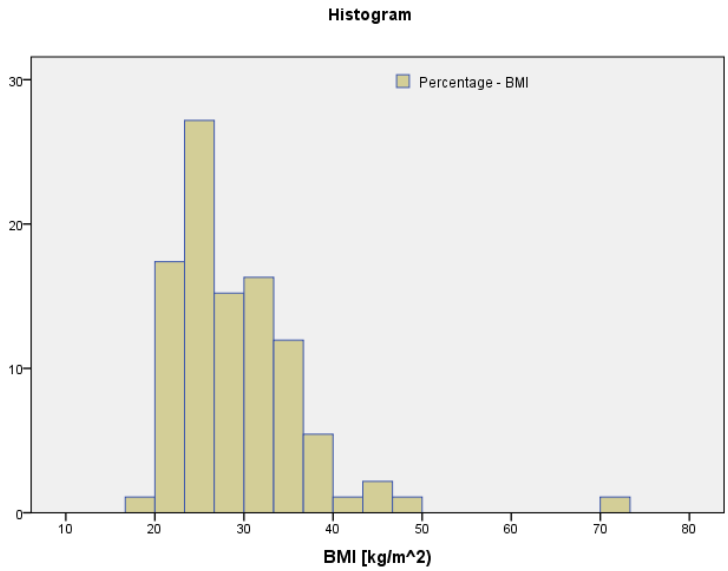

Figure 2: BMI frequency distributions over all the cohort

Radiological comparison

The non-parametric distribution analysis for each single sub-procedure are presented in tables 2, 3 and 4 . The plot, in boxplot mode, present in logarithmic scale the measured values considered for each sub-procedures.

Fluoro time (s)	Pre-update						Post-Update					
	Number	Min	1st quartile	Median	3rd quartile	Max	Number	Min	1st quartile	Median	3rd quartile	Max
ICD - New Implant - Bi-ventricular	13	127	554	804	1596	2199	13	211	597	1033	1904	5424
ICD - New Implant - Dual chamber	14	85	211	250	277	540	28	71	170	221	354	2847
ICD - New Implant - Single chamber	12	83	119	176	225	408	23	53	101	166	294	681
Permanent pacemaker - New Implant - Dual chamber	63	111	172	241	386	700	85	87	174	265	408	1840
Permanent pacemaker - New Implant - Single chamber	31	31	98	165	255	805	41	28	89	158	231	409
RFA Afib - Paroxysmal with TOE	19	1675	2297	2776	3204	4886	39	1153	1867	2181	2674	5160
RFA Atrial flutter (common type)	23	292	841	1207	1769	2923	31	416	762	957	1631	3134
RFA AV nodal slow pathway in AVNRT	38	175	346	497	696	1283	50	151	325	412	600	1606
RFA Overt accessory pathway	11	161	391	443	865	3149	24	235	503	736	1139	2420
Pacing & ICD Implant	**133**	**31**	**157**	**237**	**367**	**2199**	**190**	**28**	**142**	**231**	**390**	**5424**
RF Ablation	**91**	**161**	**452**	**799**	**1872**	**4886**	**144**	**151**	**450**	**873**	**1973**	**5160**

Table 2:Pre and Post system update - Total Fluoroscopy time per single procedure statistical comparison.

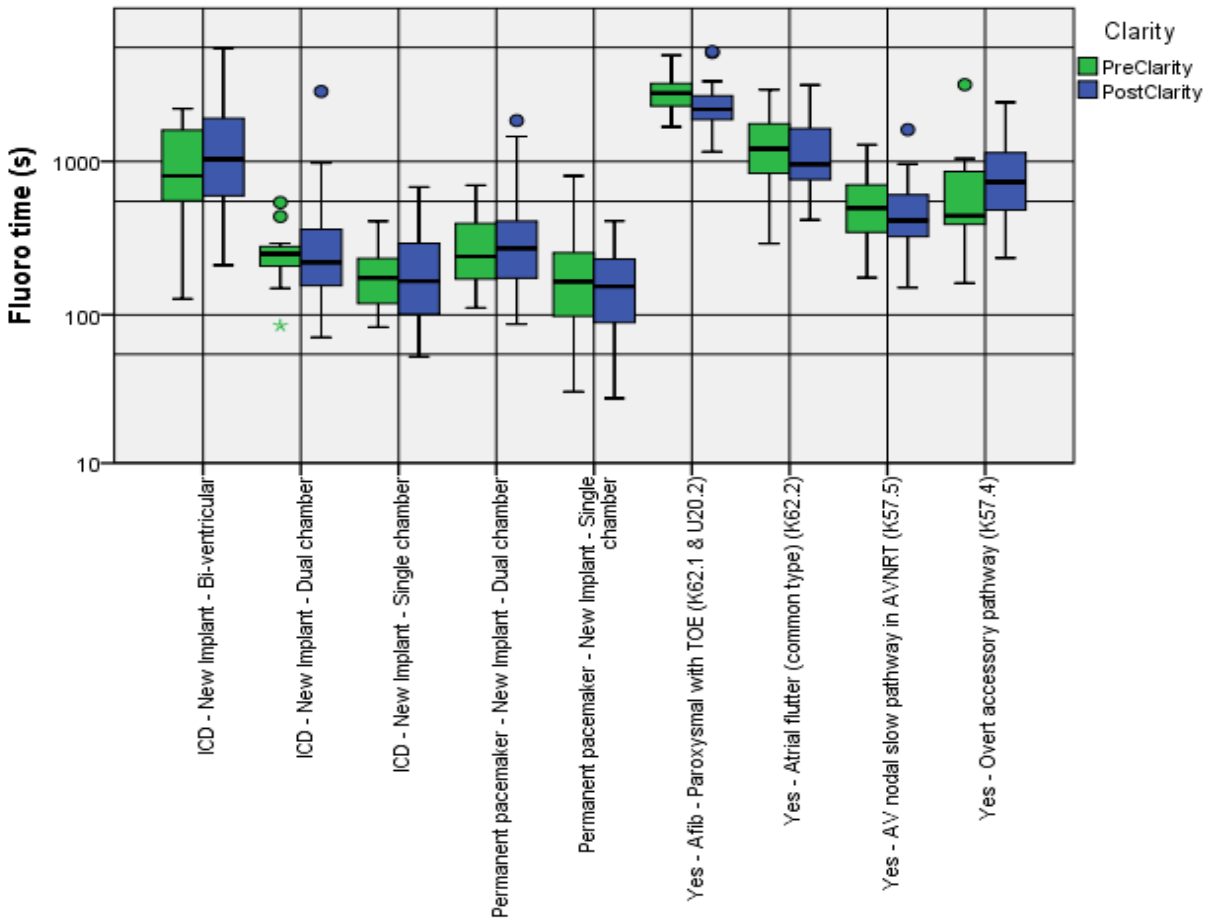

Total DAP (dGycm^2)	Pre-update						Post-Update					
	Number	Min	1st quartile	Median	3rd quartile	Max	Number	Min	1st quartile	Median	3rd quartile	Max
ICD - New Implant - Bi-ventricular	13	16	92	163	368	651	13	8	45	114	142	326
ICD - New Implant - Dual chamber	14	7	21	29	57	150	28	2	6	11	19	324
ICD - New Implant - Single chamber	12	6	13	21	25	59	23	2	6	8	9	23
Permanent pacemaker - New Implant - Dual chamber	63	5	13	24	34	149	85	2	8	13	20	236
Permanent pacemaker - New Implant - Single chamber	31	4	11	19	27	73	41	1	4	6	11	36
RFA Afib - Paroxysmal with TOE	19	144	325	423	648	1063	39	66	138	178	255	615
RFA Atrial flutter (common type)	23	42	91	153	273	631	31	15	38	52	92	365
RFA AV nodal slow pathway in AVNRT	38	11	29	63	100	406	50	6	11	17	26	100
RFA Overt accessory pathway	11	13	49	53	134	321	24	5	17	34	60	143
Pacing & ICD Implant	**133**	**4**	**13**	**24**	**44**	**651**	**190**	**1**	**6**	**10**	**19**	**326**
RF Ablation	**91**	**11**	**51**	**103**	**305**	**1063**	**144**	**5**	**20**	**48**	**135**	**615**

Table 3:Pre and Post system update - Total DAP per single procedure statistical comparison.

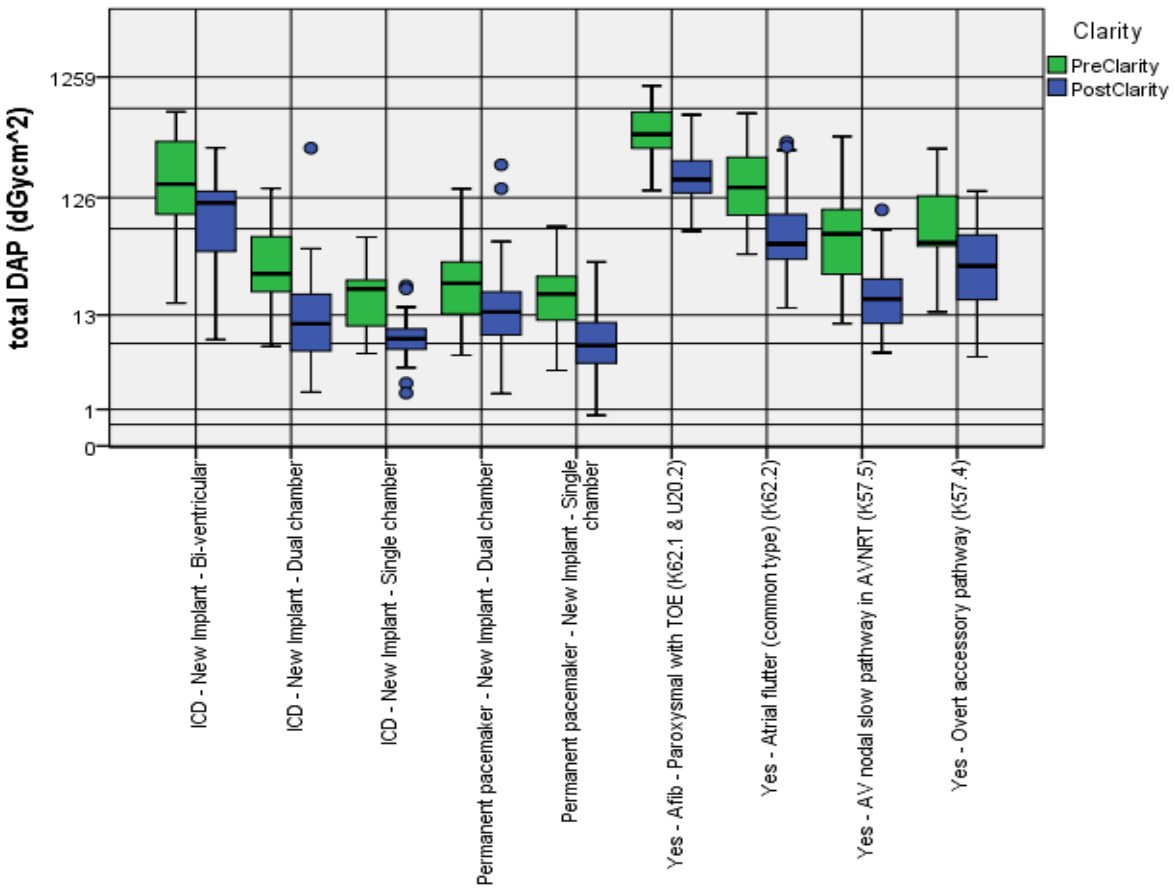

Entrance Dose (mGy)	Pre-update						Post-Update					
	Number	Min	1st quartile	Median	3rd quartile	Max	Number	Min	1st quartile	Median	3rd quartile	Max
ICD - New Implant - Bi-ventricular	13	22	75	157	409	749	13	10	63	132	161	481
ICD - New Implant - Dual chamber	14	7	22	38	65	155	28	3	8	13	23	373
ICD - New Implant - Single chamber	12	5	11	23	30	65	23	4	7	9	12	27
Permanent pacemaker - New Implant - Dual chamber	63	6	15	26	43	172	85	3	10	17	29	411
Permanent pacemaker - New Implant - Single chamber	31	6	13	20	37	95	41	2	5	8	12	50
RFA Afib - Paroxysmal with TOE	19	212	430	514	905	1463	39	133	195	222	343	1016
RFA Atrial flutter (common type)	23	53	121	186	314	853	31	21	64	84	154	553
RFA AV nodal slow pathway in AVNRT	38	19	41	86	118	563	50	7	16	27	43	108
RFA Overt accessory pathway	11	20	62	80	210	653	24	8	28	48	101	268
Pacing & ICD Implant	**133**	**5**	**16**	**28**	**51**	**749**	**190**	**2**	**8**	**14**	**26**	**481**
RF Ablation	**91**	**19**	**72**	**138**	**389**	**1463**	**144**	**7**	**29**	**72**	**195**	**1016**

Table 4:Pre and Post system update - Total Entrance Dose per single procedure statistical comparison.

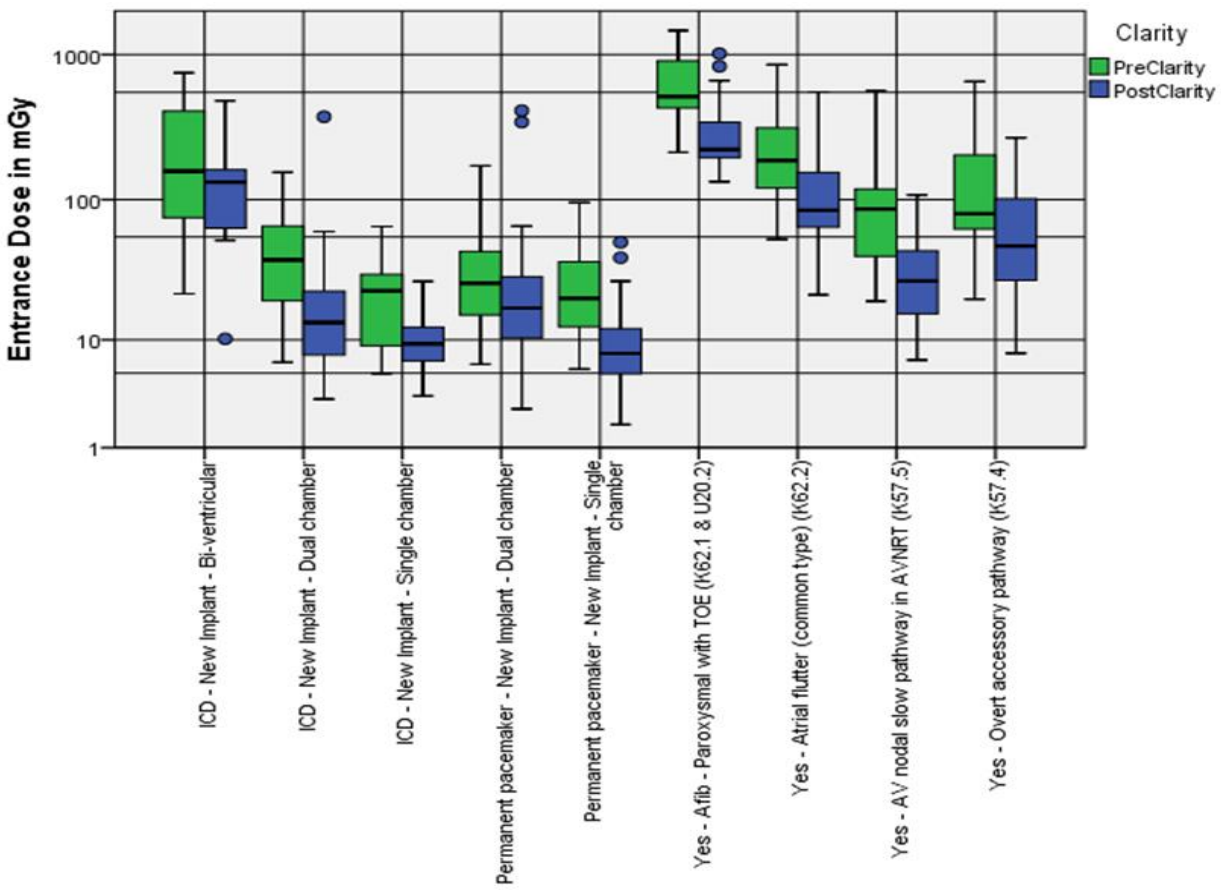

The statistical comparisons between the pre-update and post update data over the PM&ICD and RFA procedures are provided in figure 3. The confidence intervals represented in the histogram plot are evaluated with the COX method 95% confidence intervals of the mean as described in methods.

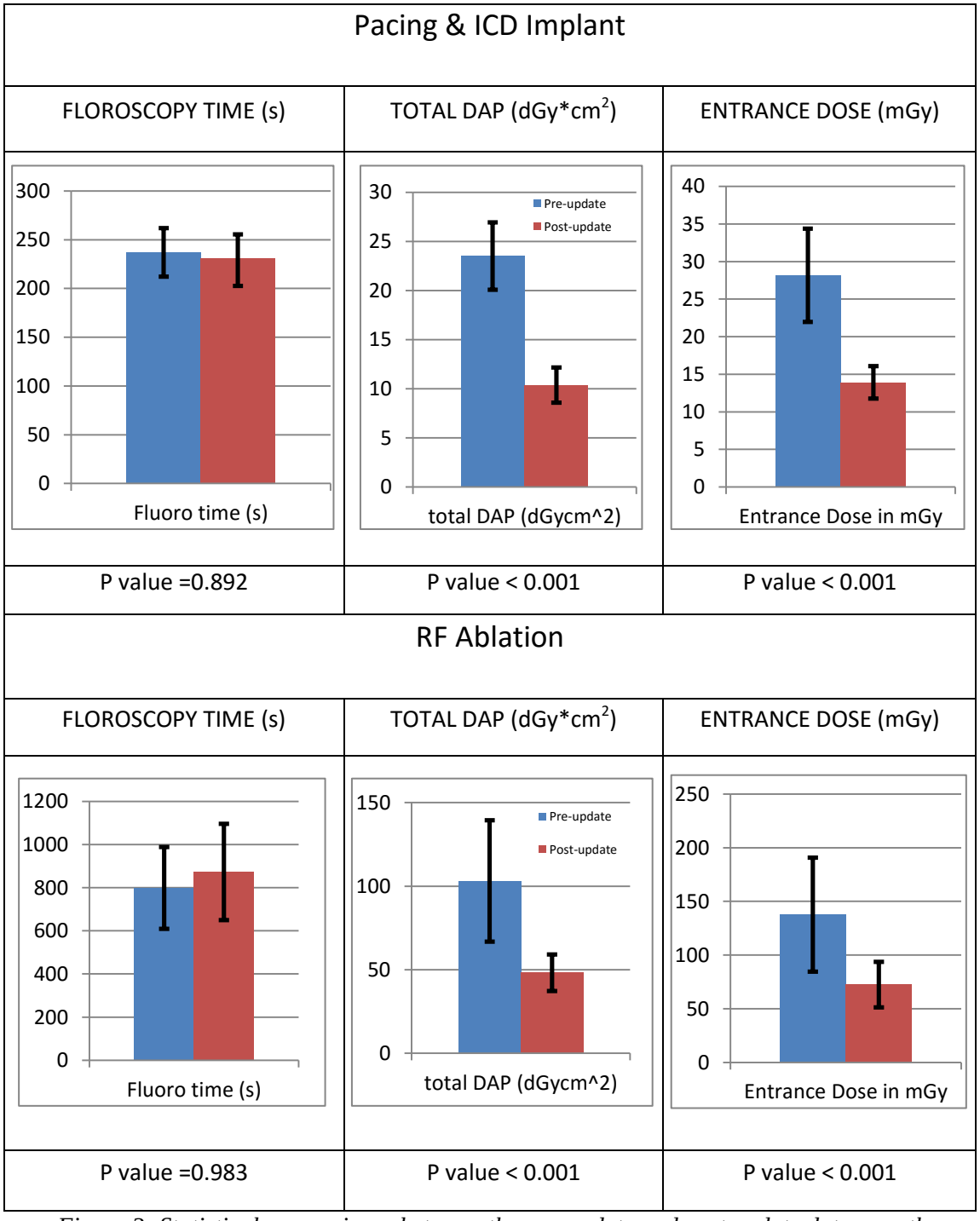

Figure 3: Statistical comparisons between the pre-update and post update data over the two main groups of procedures (PM&ICD and RF Ablation). The bar plot are evaluated with the COX method 95% confidence intervals.

The evidence of the non-normality is evaluated on single statistical test over the sample. The logarithmic behaviour of the distributions can be clearly appreciated in the Q-Q plots comparison presented in figure 4.

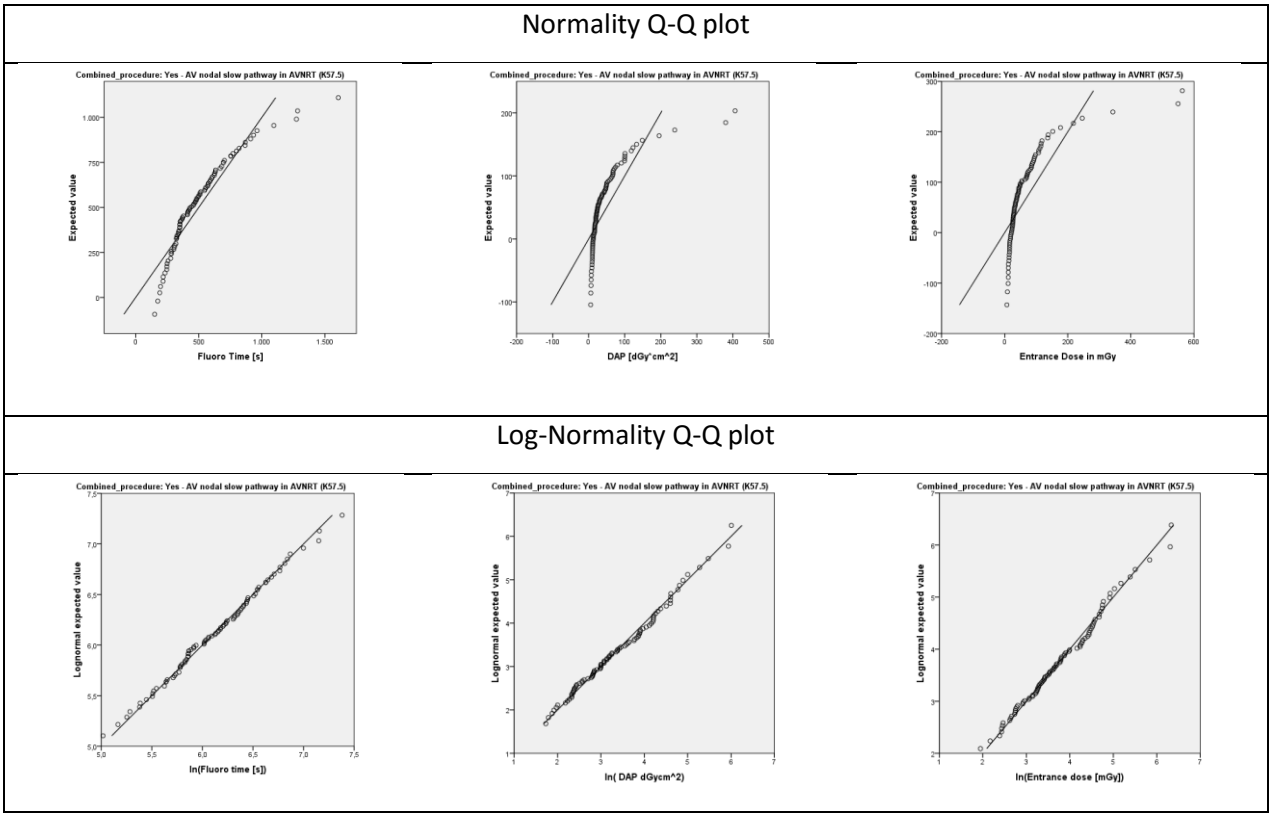

Figure 4: Q-Q Plots of the post-update data for the suprocedure RFA of AV nodal slow pathway in Atrioventricular Nodal Re-entrant Tachycardia (AVNRT);

Discussion and Conclusions

The collected data permit to evaluate the statistical significance of the variation in term or radiological data between before-update and after-update. This results has been evaluated for the fluoroscopy time ($p>0.5$) and for both the DAP and D_{AK} ($p<0.01$).

There are no significant differences between the two groups in term both of patient age and Body Mass Index (BMI) between before and after the update ($p>0.05$). The non-normal behaviour of fluoroscopy time, DAP, and D_{AK} has been proved. The lognormal fitting of the distribution of this quantities has already known in literature [18], but at the same time there is no evidence of the

physical meaning of this trend. Further investigations will be focused on the lognormal distribution in feedback proportional systems. This result, in fact, seems to be related to many other distributions in nature [19].

The comparison results shows a significant reduction of the for the DAP equal to 54% over all the procedures.

In conclusion, the analysis shows that for all the EP procedures considered the Philips Clarity update reduce significantly the patient dose without changing significantly the time of fluoroscopy: the implemented noise reduction algorithms doesn't affect the diagnostic ability of the operators.

References

1. Rossi, P. L. et al. Medical staff radiation exposure in electrophysiology procedures: First results during biventricular ICD implantation. Radiat. Meas. 46, 1228–1230 (2011).

2. Rossi Pier Luca, Bianchini David, Boni Martino, Corazza Ivan, Compagnone Gaetano, Boriani Giuseppe, Testoni, Giovanni, Z. R. Patient dosimetry during biventricular ICD insertion. Proc. Third Eur. IRPA Congr. Helsinki 1, (2010).

3. Cousins, C. et al. ICRP PUBLICATION 120: Radiological protection in cardiology. Ann. ICRP 42, 1–125 (2013).

4. Miller, D. L. et al. Occupational radiation protection in interventional radiology: a joint guideline of the Cardiovascular and Interventional Radiology Society of Europe and the Society of Interventional Radiology. J. Vasc. Interv. Radiol. 21, 607–15 (2010).

5. NCRP Report No. 168 Radiation Dose Management for Fluoroscopically--guided Interventional Medical Procedures. 2011

6. Söderman, M. et al. Radiation dose in neuroangiography using image noise reduction technology: a population study based on 614 patients. Neuroradiology 55, 1365–72 (2013).

7. Dekker, L. R. C. et al. New image processing and noise reduction technology allows reduction of radiation exposure in complex electrophysiologic interventions while maintaining optimal image quality: a randomized clinical trial. Heart Rhythm 10, 1678–82 (2013).

8. Rossi, P. L. et al. Decrease in patient radiation exposure by a tantalum filter during electrophysiological procedures. Pacing Clin. Electrophysiol. 32 Suppl 1, S109–S112 (2009).

9. Tsalafoutas, I. a et al. Radiation doses to patients and cardiologists from permanent cardiac pacemaker implantation procedures. Pacing Clin. Electrophysiol. 28, 910–916 (2005).

10. Models, N. Estimating Times of Surgeries with Two Component. 232–240 (2003).

11. Marshall, N. W., Chapple, C. L. & Kotre, C. J. Diagnostic reference levels in interventional radiology. Phys. Med. Biol. 45, 3833–46 (2000).

12. Press, C. & Sciences, B. Log-normal Distributions across the Sciences : Keys and Clues. 51, 341–352 (2014).

13. Kwon, D., Little, M. P. & Miller, D. L. Reference air kerma and kerma-area product as estimators of peak skin dose for fluoroscopically guided interventions. Med. Phys. 38, 4196 (2011).

14. Zou, G. Y., Taleban, J. & Huo, C. Y. Confidence interval estimation for lognormal data with application to health economics. Comput. Stat. Data Anal. 53, 3755–3764 (2009).

15. Zhou, X. H. & Gao, S. Confidence intervals for the log-normal mean . Stat. Med. 16, 783–90 (1997).

16. Krishnamoorthy, K. & Mathew, T. Inferences on the means of lognormal distributions using generalized p -values and generalized conÿdence intervals. 115, 103–121 (2003).

17. Bonett, D. G. & Price, R. M. Statistical inference for a linear function of medians: Confidence intervals, hypothesis testing, and sample size requirements. Psychol. Methods 7, 370–383 (2002).

18. Aroua, A., et al. "How to set up and apply reference levels in fluoroscopy at a national level." *European radiology 17.6 (2007): 1621-1633.*

19. Limpert, Eckhard, Werner A. Stahel, and Markus Abbt. "Log-normal Distributions across the Sciences: Keys and Clues On the charms of statistics, and how mechanical models resembling gambling machines offer a link to a handy way to characterize log-normal distributions, which can provide deeper insight into variability and probability—normal or log-normal: That is the question." BioScience 51.5 (2001): 341-352.

5. ACKNOWLEDGMENT AND DISCLAMERS

Because of his fundamental contribution in my PhD, and in all my academic career, this work is dedicated to Prof. Romano Zannoli and to the Medical Physics Center of the Policlinico S. Orsola Malpighi – University of Bologna.

A special thanks goes to Mr Andy Rogers and all the crew of the Health Physics Unit of the Nottingham University Hospitals NHS.

The second paper presented, on Philips Clarity System, contains data that cannot be published as a part of a project with restricted polity of publications.